Forming characteristics of the novel robot tube bending process

xunzhong Guo (guoxunzhong@nuaa.edu.cn)
Nanjing University of Aeronautics and Astronautics
zhenbiao Sun
Nanjing University of Aeronautics and Astronautics
chunmei Liu
Nanjing University of Aeronautics and Astronautics
zushu Huang
Nanjing University of Aeronautics and Astronautics
shuo Zheng
Nanjing University of Aeronautics and Astronautics
cheng Cheng
Nanjing University of Aeronautics and Astronautics
jie Tao
Nanjing University of Aeronautics and Astronautics

Research Article

Keywords: Robot tube bending, Rotary draw bending, Forming characteristics, Cross-section distortion, Finite element simulation

Posted Date: March 14th, 2022

DOI: https://doi.org/10.21203/rs.3.rs-1413481/v1

Forming characteristics of the novel robot tube bending process

Zhenbiao Sun, Chunmei Liu*, Xunzhong Guo*, Zushu Huang, Shuo Zheng, Cheng Cheng, Jie Tao

College of Material Science and Technology, Nanjing University of Aeronautics and Astronautics, Nanjing 211100, P.R. China

* Corresponding to Prof. Xunzhong Guo and Ph.D. Chunmei Liu

E-mail address: guoxunzhong@nuaa.edu.cn , liuchunmei@nuaa.edu.cn

Telephone(O): +86-13601581696; +86-15349271015

Abstract: Along with the development of “Industrial 4.0”, the application of industrial robot is becoming more and more extensive. Based on the industrial robot platform, a novel robot tube bending technology has been proposed. In order to provide guidance for the forming quality of tube bent by robot, using the plastic forming theory and simulation analysis method, compared with the rotary draw bending, the forming mechanism and characteristics of robot tube bending were analyzed. The Al6061 thin-walled tube with small diameter was taken as the research object. The results show that, in the novel robot tube bending process, since the bending die is feeding in the direction of the pipe axis while rotating, it will reduce to some extent the axial tensile stress T on the pipe during the bending process. Therefore, compared with the traditional rotary draw bending, the tensile stress and strain and thinning rate on the outer side of bent tube are both smaller, while the compressive stress and strain and thickening rate of the inner tube are instead larger in the robot tube bending process. With the increase of bending angle, the maximum cross-sectional distortion of bent tube in the robot tube bending process remains basically unchanged and is always smaller than that in the rotary draw bending process, and the greater the bending angle, the more obvious the difference. In summary, the robot tube bending technology plays a more positive role in reducing the thickness reduction and section distortion of the small diameter tube.

Keyboards: Robot tube bending; Rotary draw bending; Forming characteristics; Cross-section distortion; Finite element simulation

1 Introduction

Thin-walled hollow component with small diameter is widely used in aerospace, petrochemical, automobile, ship and other fields as structural components and fluid transport medium by virtue of its own lightweight, high performance, high efficiency and other advantages [1-3]. At present, there are many forming methods of tubular hollow components [4-6], including numerical control bending, roll bending, push bending, three-dimensional free bending, etc. Robot tube bending technology is a new forming process for small diameter thin-walled tube, which adds robot control to the tube forming process. With the advantages of high degree of freedom and accurate positioning of the robot arm, the posture and position of the end bending actuator controlled at the end of the robot arm are adjusted to ensure the accurate spatial position of the end bending actuator during the bending process, thereby improving the forming quality and forming accuracy of the tube and improving the forming efficiency.

The structure of the end forming device of the robot tube bending device is similar to that of the rotary draw bending device. However, in the bending process, the bending die in the robot tube bending device will move along the axis direction of the tube in addition to the rotation movement, while the bending die in the rotary draw bending device only rotates movement, as shown in Fig. 1.

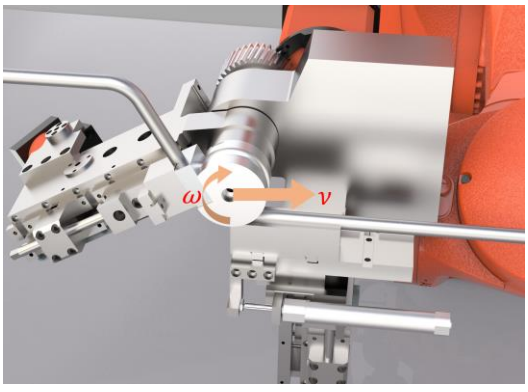

Fig. 1. The bending actuator of robot tube bending process.

In addition to the advantages of high automation and fast forming efficiency, robot tube bending technology also has a good application prospect for components with complex spatial structures. At present, the traditional numerical control bending system

cannot form the tube with multiple bifurcation branches and complex spatial configuration at one time, and it can only form the spatial shape in advance, and then connect the branches by manual welding. There are problems such as poor quality at the connection and difficult processing [7]. By using robot tube bending technology, each bifurcated branch tube can be connected to the tube in advance, and the end effector can be controlled by the robot arm to move to the desired forming position. The flexibility of the robot arm can be used to adjust the attitude of the actuator to avoid the pre-installed bifurcated branch tube, so as to realize the one-time forming of this type of complex spatial configuration tube with branch tube, which greatly improves the forming efficiency and forming quality of the tube.

The aerospace field has strict restrictions on the use of space, and the utilization rate of hollow tube components is as high as 90%. Therefore, there is a high requirement for the accuracy and quality of tube bending [8]. Tube bending is a complicated process. The common defects include thinning and rupture of outer wall thickness, thickening and wrinkling of inner wall thickness and distortion of cross section.

A large number of scholars in China and abroad have studied the traditional bending forming process: Liu et al. [9]in order to improve the prediction accuracy of bending cross-section deformation, the bending cross-section deformation of thin-walled heterogeneous rectangular welded tube considering different yield criteria was studied. The results show that Hill48 yield criterion can well describe the anisotropy of rectangular welded tube. In addition, the experimental results of Mises, Barlat and Hill48 yield criterion are compared under different bending angles and the number of core balls. It is found that Hill48 anisotropic yield criterion is the most suitable criterion for predicting the cross-section deformation of thin-walled heterogeneous rectangular welded tube. Liu et al. [10] the forming quality of thin-walled rectangular waveguide with small radius rotating drawing under different boosting conditions was studied. The changes of cross section and wall thickness were analyzed. The results show that the boosting can reduce the cross-section deformation and wall thickness reduction rate of the tube. The effect of increasing the thrust force on the section deformation of the core rod support area is less than that of the non-core rod support area, and the effect on the

wall thickness is opposite. A reasonable boost matching condition is also obtained. Che et al. [11] based on the full flow theory, the causes and control methods of the inner wrinkling and the outer wrinkling of the tube in the bending process were studied and analyzed. The stress-strain formula was established by using the theoretical analysis method, and the basis for the occurrence of the outer wrinkling and the inner wrinkling of the tube was deduced. The wrinkling occurrence formula in the bending process was proposed by using the energy criterion, and the wrinkling instability formula was determined to summarize the boundary parameters. Huang et al. [12]by establishing the finite element model of numerical control bending of Ti-3Al-2.5V titanium alloy seamless tube, the variation characteristics of tube wall thickness under different geometric parameters and process parameters were studied. Fang et al. [13]by establishing the finite element model of 21-6-9 high strength stainless steel tube with elastic modulus, the influence of process parameters on the wall thickness reduction of 21-6-9 stainless steel tube was analyzed. The results show that the elastic modulus has no obvious influence on the variation trend of wall thickness reduction, but increases its value. Li et al. [14]by analyzing the mechanism characteristics of aluminum alloy thin-walled tube with small bending radius, according to the numerical control bending process, the key technologies such as die material, die structure and finite element simulation were systematically studied. Finally, the bending forming of aluminum alloy thin-walled tube with small bending radius meeting the design requirements was realized, and the feasibility of this technology was verified. Safdarian et al. [15] based on the response surface method and the finite element method, the effects of the pressure-boosting speed of the die, the position of the mandrel, the number of mandrels and the pressure of the die on the wrinkling and cross-section distortion of the tube in the bending process were studied. The results show that the position of the mandrel is one of the main parameters affecting the cross-section distortion of the tube, and the ovality of the tube section increases with the increase of the position of the mandrel.

However, there are few studies on the robot tube bending process. Since the bending die is fixed on the spindle of the machine tool in the traditional bending, and the bending die in the robot tube bending process will have a motion in the direction

of the tube axis while rotating, the research results of the traditional bending cannot be simply applied to the robot tube bending process. The evolution law of defects in robot tube bending process during forming is not clear, especially for the study of tube, internal and external stress and strain, wall thickness thinning rate and section distortion rate. In this paper, the mechanism of robot tube bending process is analyzed based on the plastic forming principle of tube, and the calculation formula of the internal and external equivalent stress of tube is obtained. The ABAQUS finite element simulation software is used to analyze the influence of robot tube bending process and rotary draw bending process on the forming quality of tube and conduct a comparative study.

2 Mechanism analysis of robot tube bending process

2.1 Principle of robot tube bending process

The robot bending system is mainly composed of the robot system, the end bending system and the external clamping system, as shown in Fig. 2(a). The end bending system is composed of bending die, insert die, clamping die and pressure die, as shown in Fig. 2(b). In the forming process, the tube end is fixed by the external clamping system; the front end of the tube is rotated around the bending die under the constraint of the clamping die and the inserts die, and the bending die rotates at an angular speed of ω.The bending radius of the tube is the radius r of the bending die, and the pressure die remains static during the bending process. While the bending die rotates, the robot system provides a linear velocity v matching the rotation of the bending die, as shown in Eq. (1), which drives the bending die to move along the axis of the tube and realizes the flexible bending of the tube under the close cooperation of the three systems.

$$v = \omega \times r \tag{1}$$

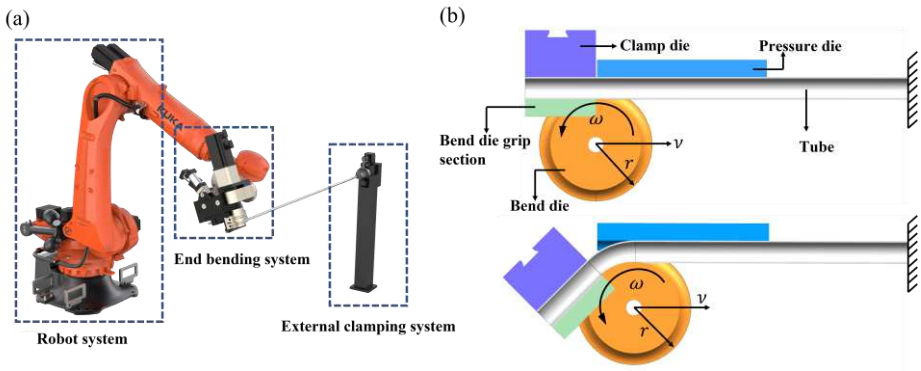

Fig. 2. Principle diagram of robot tube bending technology.

2.2 Theoretical analysis of stress and strain of tube in robot tube bending process

In the process of robot tube bending, the stress and strain state and geometric parameters of the tube subjected to the bending die, clamping block and pressure die are shown in Fig. 3, and the meanings of each symbol are shown in Table 1. Due to the tube in the bending process will produce very complex non-uniform change, in order to simplify the analysis, need to make various assumptions to approximate bending stress and strain analysis. Firstly, it is assumed that the tube conforms to the principle of constant volume in the bending process; the tangential strain, radial strain and circumferential strain of the tube are all the main strains during bending; bending tangential stress, radial stress and circumferential stress are main stress; at the same time, the plane strain state of the circumferential strain of the tube bending section is assumed.

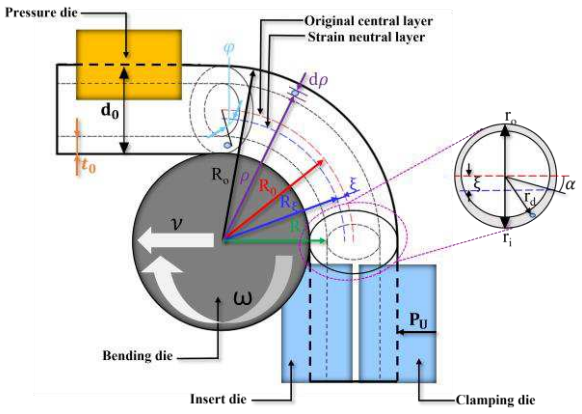

Fig. 3. Schematic diagram of stress-strain state in robot tube bending process.

Table 1 Symbols of geometric parameters and stress-strain of tube

geometric parameter	physical meaning
σ_θ、σ_β、σ_φ	Tangential stress、Radial stress、Circumferential stress
ε_θ、ε_β、ε_φ	Tangential strain、Radial strain、Circumferential strain
R_o、R_i	The outermost bending radius、The innermost bending radius
R_0	Bending radius of original neutral layer of tube
R_ξ	Bending radius of strain neutral layer of tube
α	Angle between tube radius line after strain neutral layer moving and original neutral layer radius line
φ	Angle between Cross Section Radius Line of Tube and Strain Neutral Layer
ρ	Bending radius of any point on tube
ω、v	Angular velocity of bending die 、linear velocity of bending die
P_U	Force of die on vertical tube axis

Mises plastic differential equation is expressed in Eq. (2):

$$d\varepsilon_\varphi = d\bar{\varepsilon}\left[\sigma_\varphi - (\sigma_\theta + \sigma_\rho)/2\right]/\sigma \tag{2}$$

The circumferential strain $\varepsilon_\varphi = 0$ is introduced into Eq. (2) to obtain the circumferential stress of the cross section of the bending part of the tube, as shown in Eq. (3):

$$\sigma_\varphi = \left(\sigma_\theta + \sigma_\rho\right)/2 \tag{3}$$

From the Eq. (3), the equivalent stress at the bending part of the tube is further obtained, as shown in Eq. (4):

$$\bar{\sigma} = \sqrt{\left[(\sigma_\rho - \sigma_\theta)^2 + (\sigma_\theta - \sigma_\varphi)^2 + (\sigma_\varphi - \sigma_\rho)^2\right]/2} = \sqrt{3}\left|\sigma_\theta - \sigma_\rho\right|/2 \tag{4}$$

According to the assumption that the circumferential strain of the tube is equal to 0 ($\varepsilon_{\varphi}=0$)and the volume is constant ($\varepsilon_{\rho}+\varepsilon_{\theta}+\varepsilon_{\varphi}=0$), the equivalent strain of the bending part of the tube can be expressed as Eq. (5):

$$\bar{\varepsilon}=\sqrt{2\left(\varepsilon_{\rho}{}^{2}+\varepsilon_{\theta}{}^{2}+\varepsilon_{\varphi}{}^{2}\right)/3}=2\left|\varepsilon_{\theta}\right|/\sqrt{3} \tag{5}$$

Due to the plastic deformation of most metal tubes presents a power hardening law, so this paper uses the equation that the stress-strain relationship conforms to the n-order hardening law to fit the stress-strain curve in robot tube bending process, as shown in Eq. (6):

$$\bar{\sigma}=K\varepsilon^{n} \tag{6}$$

The instantaneous strain neutral layer of the tube will move during the bending process. Assuming that the angle between the radius line of the tube after the strain neutral layer moves and the radius line of the original neutral layer is α , and $\alpha\geq 0$ is constant, the engineering strain in the tangent direction can be expressed as Eq. (7) [16]:

$$\varepsilon_{\theta}=\left(\mathrm{r}\sin\varphi+\mathrm{r}\sin\alpha\right)/\left(\mathrm{R}_{0}-\mathrm{r}\sin\alpha\right) \tag{7}$$

From Eqs. (4) - (7), we can get Eq. (8):

$$\sigma_{\theta}-\sigma_{\rho}=\pm K\left(2/\sqrt{3}\right)^{n+1}\left[\left(\mathrm{r}\sin\varphi+\mathrm{r}\sin\alpha\right)/\left(\mathrm{R}_{0}-\mathrm{r}\sin\alpha\right)\right]^{n} \tag{8}$$

Among them, in the interval $[0,\pi]$ 、 $[\pi,\pi+\alpha]$ and $[2\pi-\alpha,2\pi]$, $\mathrm{r}\sin\varphi+\mathrm{r}\sin\alpha>0$, the tangential tensile stress is generated, and the upper symbol is '+'; and in the interval $[\pi+\alpha,2\pi-\alpha]$, $\mathrm{r}\sin\varphi+\mathrm{r}\sin\alpha<0$, produce tangential compressive stress, the above symbol '-'.

Substitute Eq. (8) into Hencky stress differential equation (as shown as Eq. (7)[17]):

$$d\sigma_{\rho}/d\rho+\left(\sigma_{\rho}-\sigma_{\theta}\right)/\rho=0 \tag{9}$$

The stress equation of both sides of instantaneous strain neutral layer can be obtained as shown in Eq. (10):

$$\sigma_{\rho}=\pm K\left(2/\sqrt{3}\right)^{n+1}\left[\left(\mathrm{r}\sin\varphi+\mathrm{r}\sin\alpha\right)/\left(\mathrm{R}_{0}-\mathrm{r}\sin\alpha\right)\right]^{n}\ln\rho+\mathrm{C} \tag{10}$$

C is an integral constant. Because the radial stress at ρ=R_i and ρ=R_o sides of the tube strain neutral layer is 0, the radial stress at the inside and outside of the tube bending part can be obtained by Eq. (10), that is Eqs. (11) and (12):

$$\sigma_{\rho i}=K\left(2/\sqrt{3}\right)^{n+1}\left[\left(r\sin\varphi+r\sin\alpha\right)/\left(R_0-r\sin\alpha\right)\right]^n\ln\left(R_i/\rho\right) \tag{11}$$

$$\sigma_{\rho o}=K\left(2/\sqrt{3}\right)^{n+1}\left[\left(r\sin\varphi+r\sin\alpha\right)/\left(R_0-r\sin\alpha\right)\right]^n\ln\left(\rho/R_o\right) \tag{12}$$

Substitute Eqs. (11) and (12) into Eq. (8), the internal and external tangential stress of the tube can be obtained as shown in Eqs. (13) and (14):

$$\sigma_{\theta i}=K\left(2/\sqrt{3}\right)^{n+1}\left[\left(r\sin\varphi+r\sin\alpha\right)/\left(R_0-r\sin\alpha\right)\right]^n\left[\ln\left(R_i/\rho\right)-1\right] \tag{13}$$

$$\sigma_{\theta o}=K\left(2/\sqrt{3}\right)^{n+1}\left[\left(r\sin\varphi+r\sin\alpha\right)/\left(R_0-r\sin\alpha\right)\right]^n\left[\ln\left(\rho/R_o\right)+1\right] \tag{14}$$

The radial stress on the surface layer of the bending part is $\sigma_\rho=0$, so the equivalent stress on the innermost and outermost surfaces of the robot tube bending can be obtained from Eq. (4), as shown in Eqs. (15) and (16):

$$\bar{\sigma}_i=\left|K\left(2/\sqrt{3}\right)^n\left[\left(r\sin\varphi+r\sin\alpha\right)/\left(R_0-r\sin\alpha\right)\right]^n\left[\ln\left(R_i/\rho\right)-1\right]\right| \tag{15}$$

$$\bar{\sigma}_o=\left|K\left(2/\sqrt{3}\right)^n\left[\left(r\sin\varphi+r\sin\alpha\right)/\left(R_0-r\sin\alpha\right)\right]^n\left[\ln\left(\rho/R_o\right)+1\right]\right| \tag{16}$$

3 Establishment of finite element simulation model

The robot tube bending technology and the rotary draw bending technology are similar in terms of mold structure and different in terms of forming process. In order to ensure the accuracy of the subsequent comparative study and analysis, the same structural model is used for the finite element simulation analysis of the two forming processes in this paper.

3.1 Establishment of 3D model

The 3D finite element models of the robot tube bending and the rotary draw bending were established by UG10.0, and then imported into ABAQUS finite element simulation software, as shown in Fig. 4. The tube diameter D is 16mm, Wall thickness is 1mm, the length is 400mm, the radius of bending die is 40mm, the length of insert die and clamping die is set to 3D length, that is 50mm.

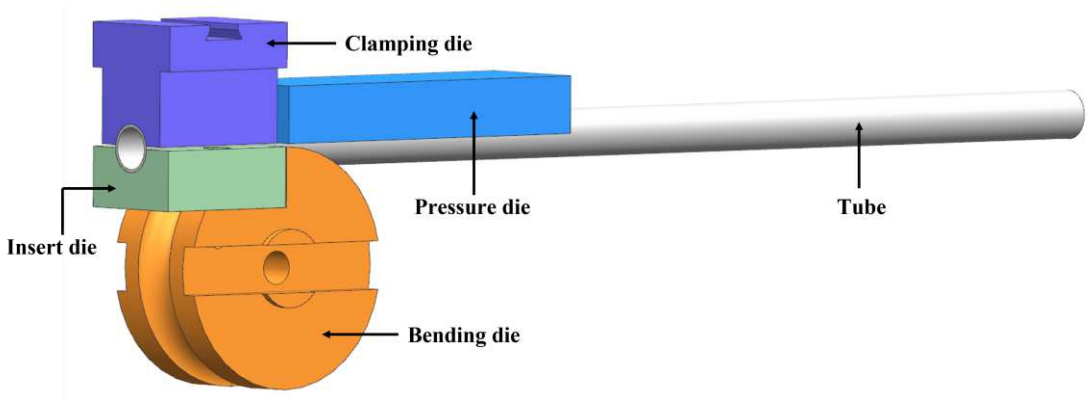

Fig. 4. 3D geometric models of each die for robot tube bending forming.

3.2 Material parameter

The mechanical properties of Al6061 alloy tube with specification of ϕ16 × 1 mm were experimentally studied, and the yield strength, tensile strength, elastic modulus, Poisson' s ratio and other parameters were obtained. The test was strictly carried out in accordance with the national standard GB/T228.1-2010 for room temperature tensile test of metal materials. Room temperature tensile tests are performed on an electronic universal testing machine, as shown in Fig. 5. The tensile strain was recorded by a longitudinal extensometer with a model of YYU-10/15 and a gauge of 15 mm. In this tensile test, the longitudinal arc specimen was adopted and intercepted along the axial direction of the tube, as shown in Fig. 6.

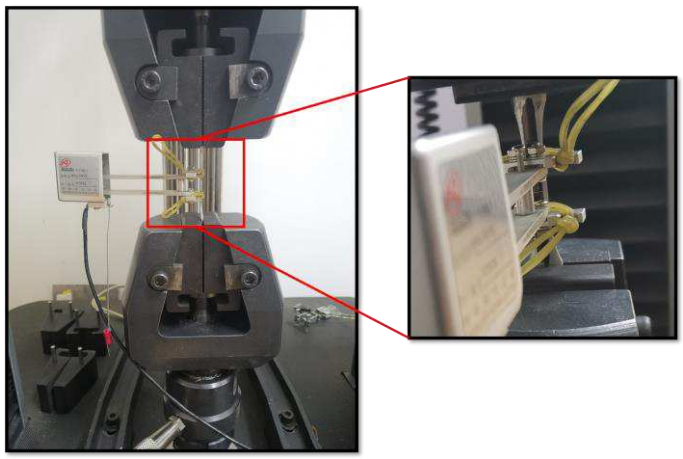

Fig. 5. Electronic universal testing machine.

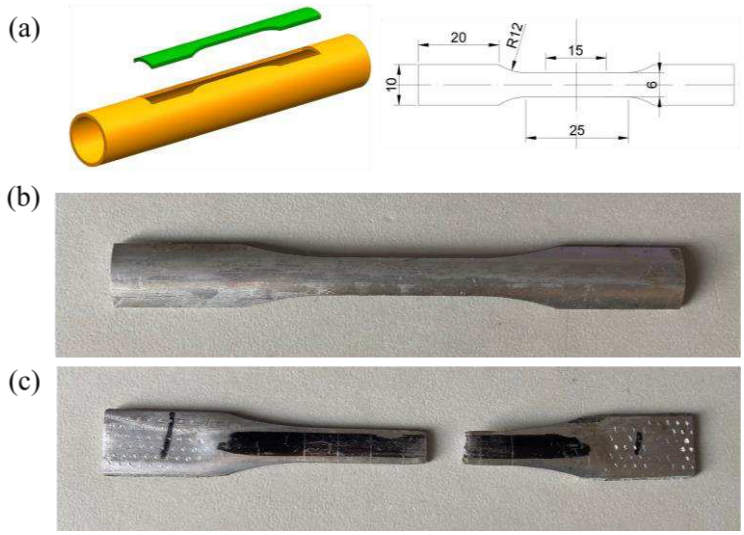

Fig. 6. Uniaxial tensile specimen: (a) geometrical dimension; (b) Before fracture; (c) After fracture.

The tensile stress-strain curve of Al6061 tube obtained by tensile test is shown in figure 7. The elastic deformation stage of the tube is obtained by fitting formula $\sigma = E\varepsilon$. The fitting starting point is the stress starting point and the end point is the yield point. The plastic deformation stage of the tube is obtained by $\sigma = K(\varepsilon + b)^n$ fitting, and the fitting range is from the yield point to the tensile limit, as shown in Fig. 7. where K is the strength coefficient of the material, n is the work hardening index, E is the elastic modulus, and b is the material constant.

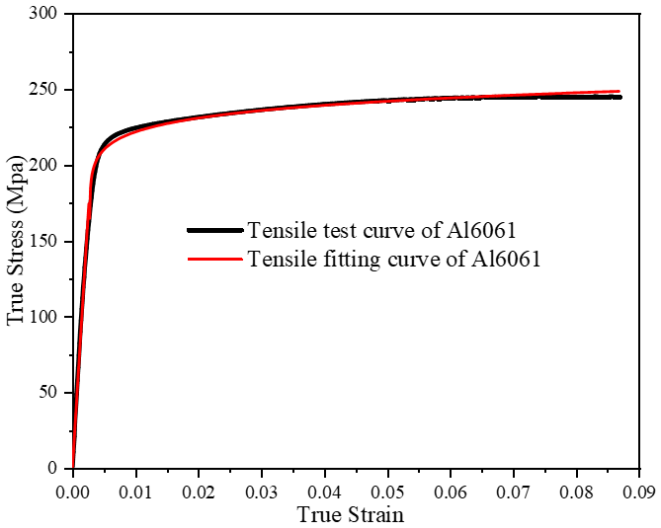

Fig. 7. True stress-strain curve of Al6061.

The material parameters of Al6061 tube obtained by the test are shown in Table 2. The elastic and plastic stage curve fitting results are shown in Eqs. (17) and (18):

$$\sigma = 72663\varepsilon \tag{17}$$

$$\sigma = 273.1144(\varepsilon - 0.00336)^{0.03947} \tag{18}$$

Table 2 The main material parameters of Al6061

Material parameters	Results
Elastic modulus (E/MPa)	72663
Poisson ratio (μ)	0.33
Yield strength ($\sigma_{0.2}$/MPa)	212
Tensile strength (σ_b/MPa)	245
Strength factor (K/MPa)	273.1144
Cementation index (n)	0.03947
Elongation (V/%)	15.5
Material constant (b)	-0.00336

3.3 Settings of key parameters

In the process of robot tube bending and rotary draw bending, the change of die is very small and can be ignored. In order to simplify the model and save computer simulation time, the die is set to discrete rigid body and described by R3D4. The discrete rigid body material does not deform. In order to improve the calculation accuracy, the tube is set to S4R shell element with deceleration integral and sand leakage control properties, and the shell thickness is 1 mm, as shown in Fig. 8.

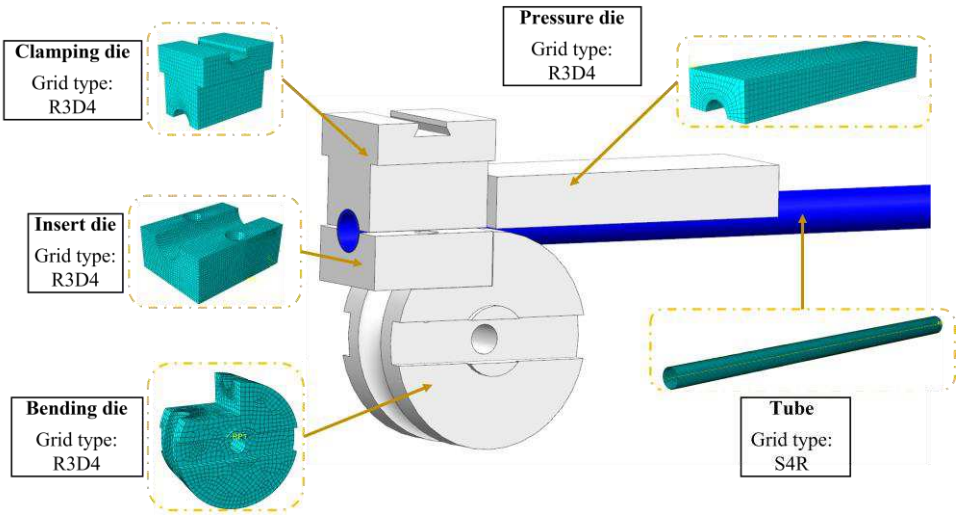

Fig. 8. Mesh division of finite element model.

The contact mode between the die and the outer surface of the tube is surface-surface contact, and the contact friction formula in the tangential direction is calculated by penalty function. The friction coefficient between the bending die, the insert and the outer surface of the tube is 0.05, and the friction coefficient between the clamping block and the outer surface of the tube is set to infinity, so as to prevent the phenomenon of clamping failure in the bending process. The friction coefficient between the pressure die and the outer surface of the tube is 0.1. Set stress interference to ' hard ' contact in normal behavior. In order to reduce the influence of inertia effect on the simulation results in the simulation process, the amplitude curve in the bending process adopts the smooth curve.

The boundary conditions and load setting of robot tube bending process, as shown in Fig. 9(a): create the boundary conditions of 'speed/angular velocity' in the dynamic display analysis step, select the reference point of the bending die rotation center, set the rotation degree of freedom UR3 on the Z axis and the moving degree of freedom $U2$ in the Y positive direction, and the remaining degrees of freedom $U1=U3=UR1=UR2=0$;the boundary conditions of clamping block and insert block are the same as those of bending die; the tube and the pressure die are always fixed, and all degrees of freedom are constrained, that is, $U1=U2=U3=UR1=UR2=UR3=0$.

The boundary conditions and load settings of the rotary draw bending process, as

shown in Fig. 9(b): the bending die of the rotary draw bending process can rotate around the reference point, so only the rotation freedom UR3 of the open Z axis is needed, and the freedom degrees are 0, that is, $U1=U2=U3=UR1=UR2=0$; the press block moves forward along the tangential direction of the tube to set the moving freedom $U2$ in the positive direction of the Y axis, and the other freedoms are 0, that is, $U1=U3=UR1=UR2=UR3=0$.

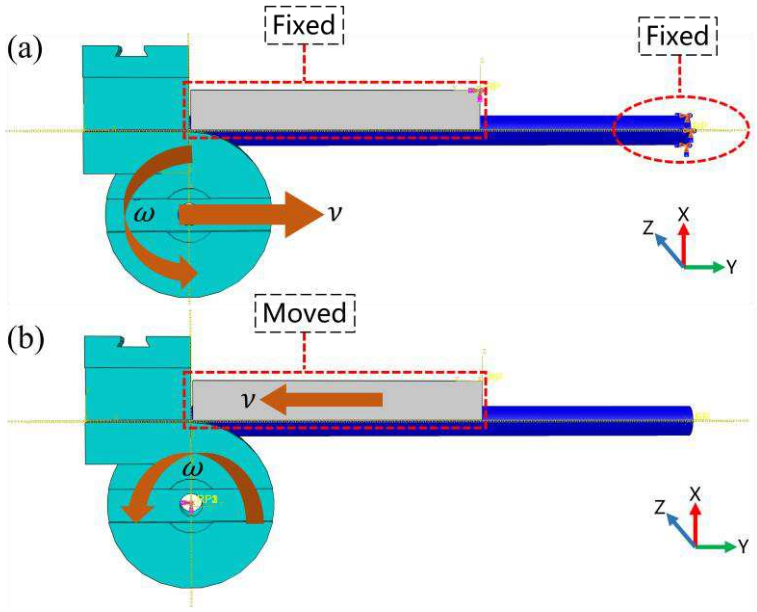

Fig. 9. Load setting: (a) Diagram of load setting in robot tube bending process; (b) Diagram of load setting in rotary draw bending process.

Tube mesh is divided by hexahedron structure, the number of circumferential direction mesh is 20, the number of axial direction mesh is 200. Because the mold is a discrete rigid body, in order to improve the efficiency of finite element simulation, the mesh size of the mold part is 3 mm, and the maximum deviation factor is 0.1. In order to ensure the calculation efficiency in the simulation process, the 10000mass scaling coefficient can reduce the calculation time and ensure the quality of the simulation.

3.4 Reliability verification of finite element simulation

In order to ensure the accuracy and reliability of the subsequent analysis, it is necessary to test the above established robot tube bending finite element model and rotary draw bending finite element model. Based on the prototype of robot tube bending principle developed and the numerical control bending machine (as shown in Fig. 10),

the tube bending verification test is carried out. The accuracy and reliability of the finite element model are judged by comparing the error of wall thickness thinning and section distortion between the tube formed in actual test and the tube formed in simulation. Table 3 is the condition parameters of simulation and experimental forming:

Table 3 Experimental and simulated bending condition parameters

Process	Robot tube bending		Rotary draw bending	
Parameter	Simulation	Experiment	Simulation	Experiment
Diameter/ (mm)	16	16	16	16
Wall thickness /(mm)	1	1	1	1
Bending radius /(mm)	40	40	40	40
Bending angle / (°)	90	90	90	90
Bending velocity /(rad • s^{-1})	0.5	0.5	0.5	0.5
Feeding speed of bending die /(mm • s^{-1})	20	20	——	——
Pressure die advancing speed /(mm • s^{-1})	——	——	20	20
Friction coefficient between pressure die and tube	——	——	0.1	Dry friction
Friction coefficient between bending die and tube	0.05	Dry friction	0.05	Dry friction
Friction coefficient between clamp die and tube	Infinity	Carved pattern	Infinity	Carved pattern

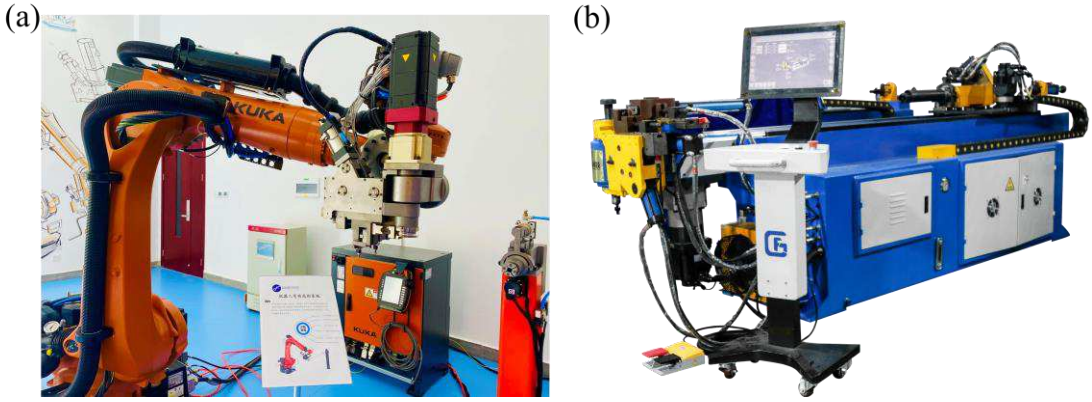

Fig. 10. Experimental equipment：(a) Robot bender machine; (b) Rotary draw bending machine.

Fig. 11(a) and (b) is the comparison of test and simulation results of robot tube

bending. Fig. 11(c) and (d) is the comparison curve of the wall thickness reduction rate and section distortion rate of the tube under different measurement angles. The measurement angle is the angle between the measurement plane and the bending plane, which is measured once every 5°. It can be seen from Fig. 11(c) that the wall thickness thinning rates of different bending parts of the tube obtained by experiment and simulation are similar, and the relative error is about 4.18 %. The relative error of the cross-sectional distortion rate of the tube tested and simulated in Fig. 11(d) is about 11.7 %, indicating that the established finite element model for bending forming of 6061 aluminum alloy tube robot is reliable. Fig. 12(a) and (b) is the comparison between the experimental results and the simulation results of the rotary draw bending. It can be seen from Fig. 12(c) and (d) that the wall thickness thinning rate and section distortion rate of the simulation and test are very close. The relative error of wall thickness thinning rate is about 5.08 %, and the error of section distortion rate fluctuates around 14.29 %, indicating that the established finite element model of rotary draw bending is accurate. In summary, the robot tube bending finite element model and the rotary draw bending finite element model established in this paper can accurately reflect the plastic forming process of tube, and can be used to study the influence of these two forming processes on the forming quality of tube.

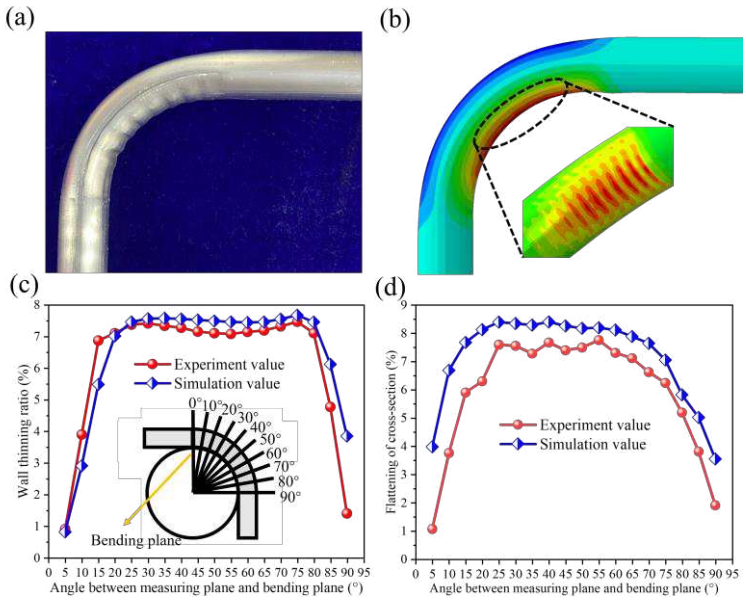

Fig. 11. Robot tube bending results: (a) Experimental results; (b) Finite element simulation results; (c) Comparison chart of wall thinning ratio; (d) Comparison chart of flattening of cross-section.

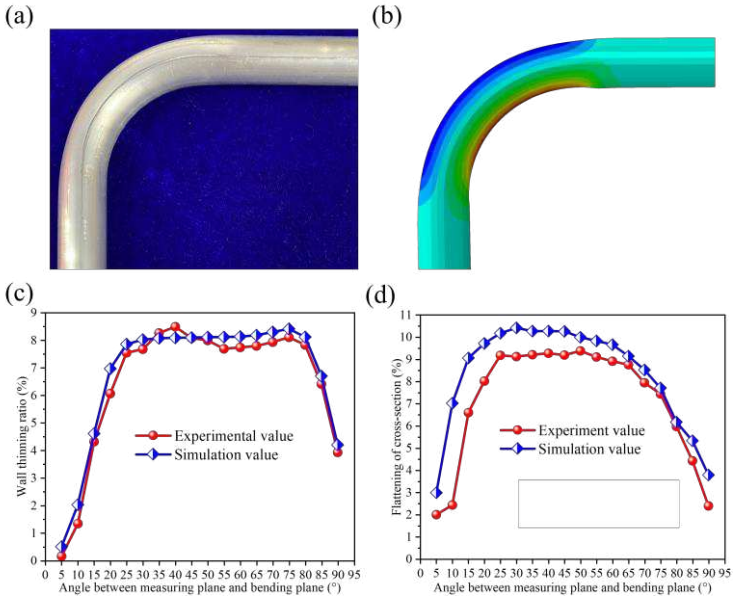

Fig. 12. Rotary draw bending results: (a) Experimental results; (b) Finite element simulation results; (c) Comparison chart of wall thinning ratio; (d) Comparison chart of flattening of cross-section.

4 Analysis of finite element simulation results

4.1 Analysis of internal and external stress and strain of tube

4.1.1 Stress comparison analysis

In the process of tube bending, the outer side of the bending will be subjected to tensile stress, and the inner side of the bending will be subjected to compressive stress. When the outer and inner stress is too large, it will cause defects such as thinning of the outer wall thickness, wrinkling of the inner side and section distortion. Fig. 13 is the equivalent stress change cloud diagram of the two forming methods of 90 ° tube. Fig. 14 shows the comparison curves of equivalent stress inside and outside the robot tube bending process and the rotary draw bending process. It can be seen that similar plastic deformations occurred in the bent tubes of robot tube bending and rotary draw bending, mainly concentrated near the bending shear point, in Fig. 13. With the continuous bending of the tube, When the measurement angle exceeds 25°, the plastic deformation area of the two gradually tends to be stable, and the tube enters a stable plastic forming stage.

The comparison curve of the equivalent stress on the outer side of the tube is

shown in Fig. 14(a). In the initial stage of bending, the equivalent stress on the outer side of the tube gradually increases with the increase of the bending angle. With the increase of bending angle, the tangential stress of the tube is in a relatively stable stage, and the ' platform ' feature appears. In this stage, the equivalent stress of the robot tube bending process is lower than that of the rotary draw bending. When the bending angle of the tube is further increased, the equivalent stress of the tube decreases, and the equivalent stress of the robot tube bending process decreases rapidly. This is because the bending die be moved along the axial direction of the tube during the bending process, which promotes the stress in the deformed area to move and diffuse to the non-deformed area, the stress is unloaded and the stress decreases. In addition, the pressure die and the tube remain stationary, there is no relative friction and the tube is not subjected to additional tangential tension T, which also reduces the external stress to a certain extent.

Fig. 14(b) shows the comparison curve of equivalent stress inside of the tube. It can be seen from the figure that there is little difference in the inner stress of the tube between the robot tube bending process and the rotary draw bending process. When the measurement angle exceeds 45°, the internal equivalent stress of the two forming processes begins to decrease, and the internal stress of the robot tube bending process decreases faster. The reason is that in the initial stage of bending, the bending deformation of the tube is not very large, and the additional tangential tension T of the rotary draw bending process has a certain positive effect on alleviating the internal stress of the tube. However, with the increase of tube bending angle, the effect of additional tangential force decreases gradually, and with the axial feed motion of the bending die of the robot tube bending process, the stress inside the tube decreases faster and the value is smaller.

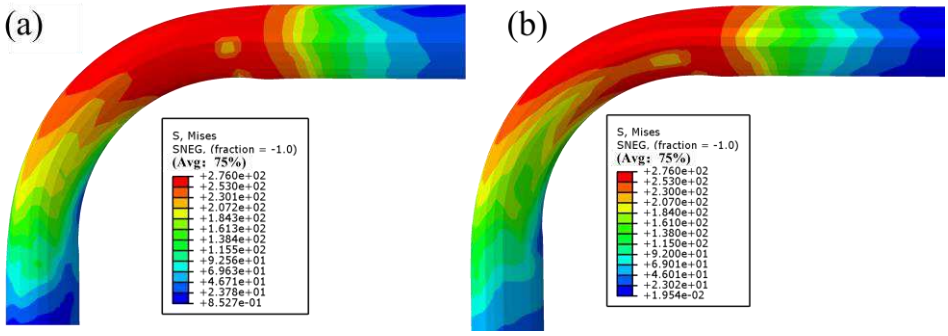

Fig. 13. Cloud chart of equivalent stress during different bending process: (a) Robot tube bending process; (b) Rotary draw bending process.

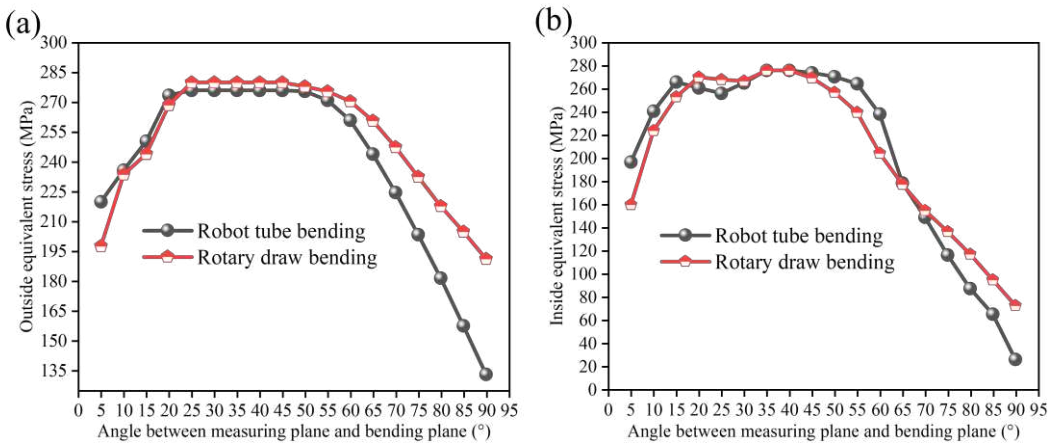

Fig. 14. Comparison diagram of internal and external equivalent stress during different bending process: (a) External equivalent stress; (b) Internal equivalent stress.

From the above comparative analysis, it can be seen that the robot tube bending process has less stress on the outer side of the tube than the rotary draw bending process, and the inner stress is larger. With the increase of tube bending angle, the stress drop rate of inner and outer tube in robot tube bending process is faster than that in rotary draw bending process.

4.1.2 Strain comparative analysis

Fig. 15 shows the tangential strain contours of the tube using the robot tube bending process and the rotary draw bending process when the tube is bent to 90°. The left side is the cloud chart of tangential strain change during the tube bending process of robot tube bending process, and the right side is the cloud chart of tangential strain change during the tube bending process of rotary draw bending process. It can be seen from the figure that with the continuous bending, the tangential strain value of the tube gradually

increases and the range gradually expands to the bending direction of the tube. The tangential compressive strain value inside the tube is greater than the tangential tensile strain value outside the same angle. The outer tensile strain of robot tube bending process is less than that of rotary draw bending process, and the tangential strain distribution range is slightly smaller than that of rotary draw bending process. The main reason is that the bending die feeds along the axial direction of the tube in the robot tube bending process, so the material is easier to flow. When the plastic deformation occurs due to the tangential tensile stress on the outer side of the tube during the clamping rotation of the clamping die, the material in the deformation area is supplemented in time under the action of the bending die feed, so that the tangential tensile strain on the outer side is reduced. At the same time, the material flow distribution is more uniform and the tangential strain distribution range is reduced in the process of bending die feeding. The tangential compressive strain value of the inner side of the tube in the robot tube bending process is slightly larger than that in the rotary bending forming process. This is because the additional tangential tension in the rotary bending forming process can alleviate the inner stress of the tube.

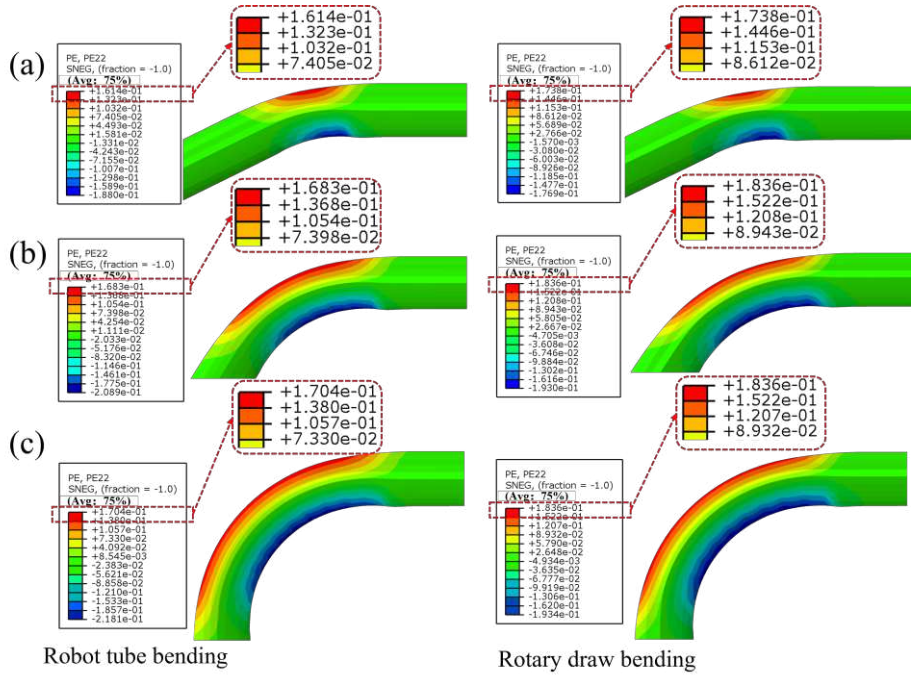

Fig. 15. The distribution of tangential strain of tube under different bending angles by two forming processes: (a)30°; (b) 60°; (c) 90°.

Fig. 16 shows the comparison curves of tangential strain distribution inside and outside the tube at different measurement angles when the bending angle is 90°. On the figure, the strain value is positive outside the tube, belonging to tensile strain; the strain value is negative inside the tube, belonging to compressive strain. It can be found from Fig. 16 that the strain at the beginning and end of tube bending deformation is small, and the deformation in the middle area of deformation is large. The tensile strain on the outer side of the tube shows a platform-shaped, indicating that the outer side is in a stable plastic deformation stage, while the compressive strain on the inner side fluctuates up and down, indicating that wrinkling occurs on the inner side of the tube. The fluctuation of the robot tube bending process is large, indicating that the wrinkling phenomenon is more obvious than that of rotary draw bending . From Fig. 16, it can be more intuitive to see that the tube is bent under the robot tube bending process, and the lateral tangential tensile strain is smaller than that of the rotary draw bending process, which is consistent with the law obtained from the tangential strain distribution diagram in Fig. 15. The tangential compressive strain of the inner side is slightly larger than that of the rotary draw bending process, which is also in line with the comparison results of the inner stress of the tube.

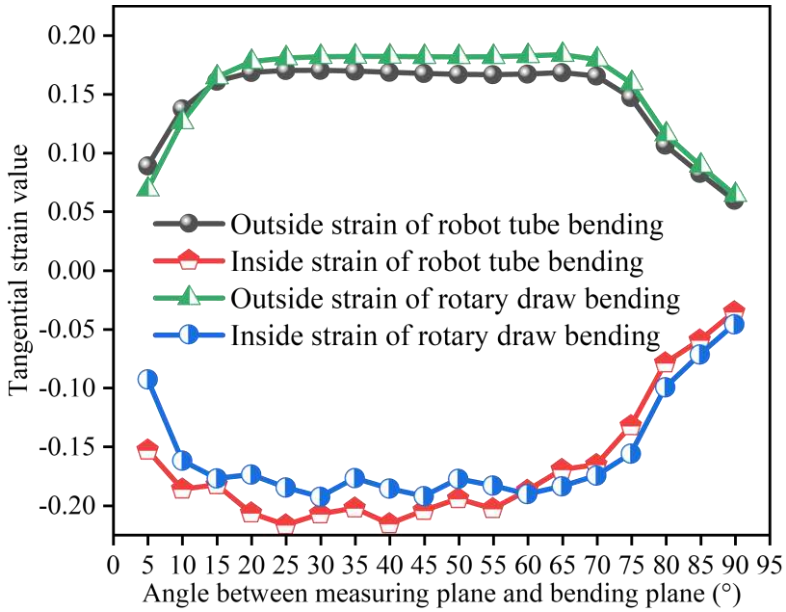

Fig. 16. The variation curve of the tangential strain inside and outside the tube along the measurement angle.

4.2 Comparative analysis of tube forming quality

Tube bending itself belongs to a complex nonlinear physical forming process under the coupling of various die structures and conditions [18]. The common indicators to measure the forming quality of tubes are the thinning rate of the outer wall thickness and the distortion rate of the cross section. The quality of these two indicators directly affects the forming quality of tubes and subsequent use. Fig. 17 shows the cross-sectional distortion of the tube and the thinning of the outer wall thickness.

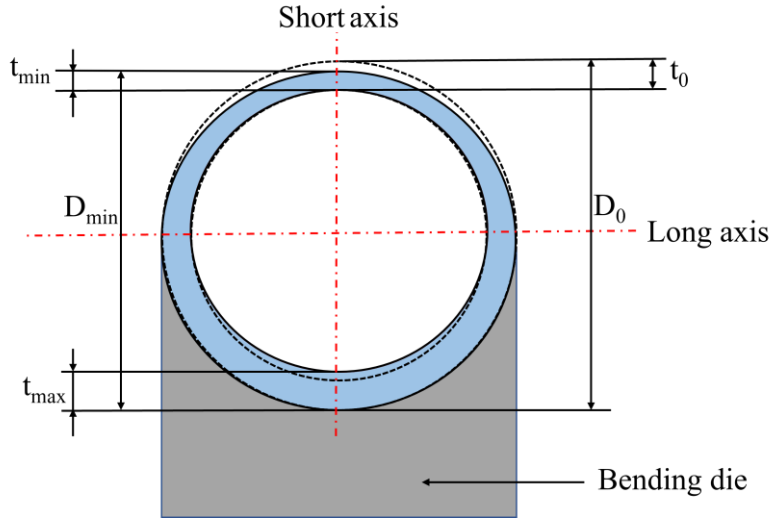

Fig. 17. Diagram of wall thickness variation and cross section distortion of bent tube.

The thinning degree of outer wall thickness of tube is generally expressed by the change rate of wall thickness before and after bending, that is, the change rate of wall thickness (δ), as shown in Eqs. (19) and (20):

$$\delta_{out} = \left[\left(t_0 - t_{min} \right) / t_0 \right] \times 100\% \tag{19}$$

$$\delta_{min} = \left[\left(t_{max} - t_0 \right) / t_0 \right] \times 100\% \tag{20}$$

where t_0 is the original wall thickness of the tube, unit mm; t_{min} is the wall thickness behind the bending, unit mm; t_{max} is the inner wall thickness after bending, unit mm.

Since the tube bending is carried out under the constraints of the mold, although the bending of the radial pressure can make the vertical direction, that is, the long axis direction of the tube diameter increases, but will be limited by the bending die groove actual change is very small, so the section distortion rate ϕ is usually calculated using

the short axis [16]. The calculation formula is shown in Eq. (21):

$$\phi = \left(D_0 - D_{min}\right)/D_0 \tag{21}$$

D_0 is the original diameter of the tube, D_{min} is the outer diameter of the short axis direction after bending.

4.2.1 Comparative analysis of wall thickness change of tube

Fig. 18(a) is a comparison of the outer wall thickness reduction rate of the tube under the two forming processes. It can be seen from the figure that in the initial stage of measurement, the outer wall thickness reduction rate of the tube increases rapidly. With the increase of the measurement angle, the outer wall thickness reduction rate of the tube enters a relatively stable stage, and a 'platform' appears. This is because with the continuous tube bending, tube plastic deformation will enter a stable deformation stage, the wall thickness will change evenly, so the wall thickness reduction rate will appear 'platform' characteristics. It can be seen from the figure that the outer wall thickness reduction rate of the tube of the robot tube bending process is about 7.3 %, and the outer wall thickness reduction rate of the tube of the rotary draw bending process is about 8.2 %. The reason is that the equivalent stress value of the outer side of the tube represented by Fig. 14(a) is different. The tangential equivalent stress value of the outer side of the robot tube bending process is small. During the bending process of the tube, the smaller the tangential stress is, the smaller the influence on the wall thickness reduction of the tube is. Therefore, the wall thickness reduction rate of the robot tube bending process is smaller than that of the rotary bending forming process.

Fig.18 (b) is the comparison chart of the thickening rate of the inner wall thickness of the tube. It can be clearly seen from the figure that the thickening rate of the inner wall thickness of the tube under the robot tube bending process is greater than that of the rotary bending forming process. The thickening rate of the inner wall thickness of the robot tube bending process fluctuates around 19%, while the rotary draw bending process fluctuates around 17%. This is because the additional tangential tension T in the rotary bending forming process has a certain positive effect on reducing the compressive stress on the inner side of the tube, which alleviates the thickening change

of the inner wall and makes the thickening rate of the inner wall relatively low. It can also be seen from the figure that the area with large difference in wall thickness thickening rate is 20° ~ 60°, that is, the area with large plastic deformation of the tube. The thickening rate of the tube in the end bending deformation area is almost the same. In these two forming methods, the thickening rate curves of the inner side wall thickness of the tube fluctuate up and down, indicating that wrinkling occurs in the inner side of the tube under the two forming processes, which is consistent with the conclusion obtained in Fig. 16.

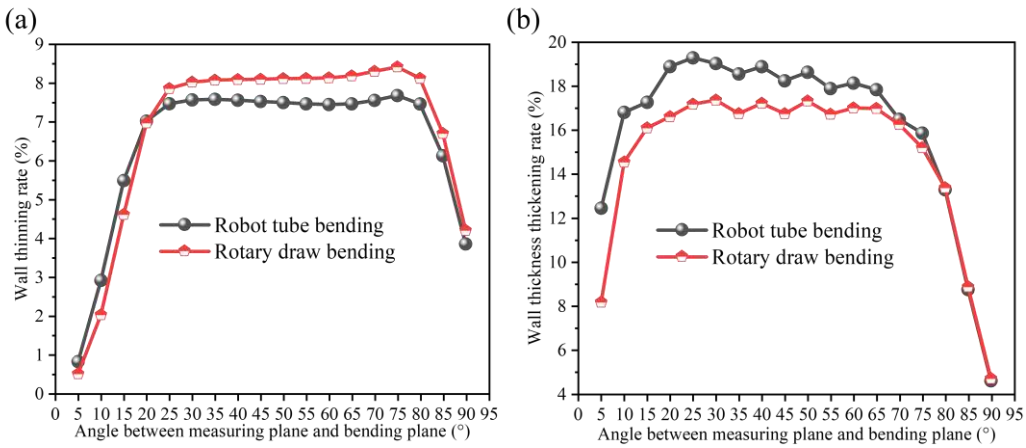

Fig. 18. Effect of two processes on wall thickness variation: (a) Wall thinning rate; (b) Wall thickness thickening rate.

4.2.2 Comparative analysis of tube cross-sectional distortion

In order to obtain the change of the cross section of the tube in the bending process more clearly, a measurement plane is set at every 10° interval in the tube bending interval, which is denoted as S1, S2, S3……S10, where S1 is the bending start plane and S10 is the bending end plane, as shown in Fig. 19. Fig. 20 is the cross-sectional distortion ratio comparison chart of the tube in different bending angles and measuring planes under two forming processes. The real line represents the robot tube bending process, and the virtual line represents the rotary draw bending process. From the diagram, it can be seen that the cross-section distortion rate of the tube formed by the robot tube bending process and the rotary bending forming process gradually increases with the increase of the bending angle, but the increase rate gradually decreases until it tends to be stable. The cross-section distortion rate of the tube formed by the robot tube

bending process is stable at about 8 %, and the cross-section distortion rate of the tube formed by the rotary draw bending process is stable at about 10%. This is because in the initial stage of the tube bending, the friction between the die and the tube, the contact state and other interactions do not reach the equilibrium and stable state. The increase of the bending angle has a great influence on the tangential stress affecting the cross-sectional deformation of the tube, and the cross-sectional distortion rate shows an upward trend. When the interaction reaches a stable state, the bending angle has little effect on the stress, so that the section distortion rate tends to be stable. In addition, when the bending angle of the tube is the same, the cross-sectional distortion rate of the tube under the robot tube bending process is smaller than that of the rotary draw bending process, and with the increase of the bending angle, the difference between the maximum cross-sectional distortion rate of the two forming processes will gradually increase. When the bending angle is 90° and the measurement plane is S4, the difference between the two cross-sectional distortion rates is the largest, about 2.01%.

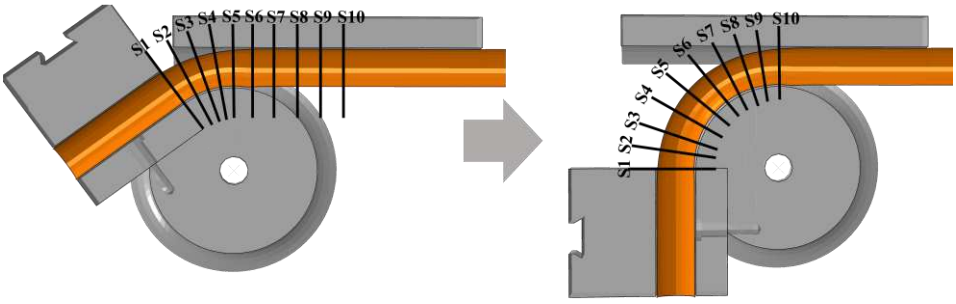

Fig. 19. The schematic diagram of the measured cross-sections.

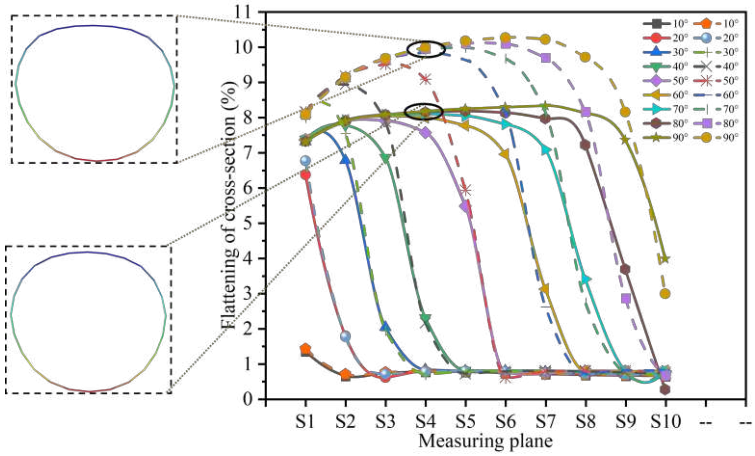

Fig. 20. Comparison of cross-section distortion during the robot tube bending and rotary draw bending process.

5 Conclusions

A novel robot tube bending technology has been proposed in this paper. In order to explore the forming characteristics of the novel robot tube bending process, based on the finite element simulation and experiment, the differences of the stress and strain, wall thickness and cross-sectional distortion of the bent tube between the novel robot tube bending and the rotary draw bending are compared and analyzed, and some conclusions are drawn:

(1) Compared with the rotary draw bending process, The robot system controls the movement of the bending die along the axis of the tube during bending die rotation, which has a positive effect on reducing the outer tangential stress of the tube.

(2) The outer tensile strain of bent tube during the robot tube bending process was smaller than that in the rotary draw bending process. While the inner strain fluctuated during the robot tube bending process, which indicated that the inner side of the tube appeared wrinkling phenomenon easily. This analysis is also verified.

(3) Compared with the rotary draw bending process, the thinning rate of the outer tube is smaller, while the thickening rate of the inner tube is larger in the robot tube bending process.

(4) With the increase of bending angle, the cross-sectional distortion ϕ of bent tube in the robot tube bending process was always smaller than that in the rotary draw bending process. When the bending angle was larger than 30 degrees, the maximum ϕ remained basically unchanged in the robot tube bending process, and the difference of the maximum ϕ under the two forming processes also increased with the increase of bending angle, the maximum difference is about 2.01 %.

(5) The robot tube bending technology plays a more positive role in reducing the thickness reduction and section distortion of the bent tube than the traditional rotary draw bending. That means it has great application potential in the precise plastic processing of small diameter thin wall tube.

Declarations

Availability of data and materials

All data generated or analysed during this study are included in this published article [and its supplementary information files].

Competing interests

The authors declare that they have no competing interests

Funding And Acknowledge

The authors would like to thank the Fundamental Research Funds for the Central Universities (No. NS2021046), National Natural Science Foundation of China (No. 52105362 and U1937206), Natural Science Foundation of Jiangsu Province (No. BK20210310).

Authors' contributions

Szb analyzed the robot bending theory, established a finite element simulation model, and completed the manuscript； Hzs and Zs handled the relevant experimental data； Lcm and Cc provided help on finite element simulation; Gxz and Tj provided experimental help.

References

[1] Cheng C, Chen H, Guo JX, Guo XZ, Shi YJ. (2021). Investigation on the influence of mandrel on the forming quality of thin-walled tube during free bending process. Journal of Manufacturing Processes, 72, 215-226. http://dx.doi.org/10.1016/j.jmapro.2021.10.018.

[2] Li H, Ma J, Liu BY, Gu RJ, Li GJ. (2018). An insight into neutral layer shifting in tube bending. International Journal of Machine Tools and Manufacture, 126, 51-70. http://dx.doi.org/10.1016/j.ijmachtools.2017.11.013.

[3] Song HW, Xie WL, Zhang SH, Jiang WH, Lăzărescu L, Banabic D. (2021). Granular media filler assisted push bending method of thin-walled tubes with small bending radius. International Journal of Mechanical Sciences ,198.http://dx.doi.org/10.1016/j.ijmecsci.2021.106365.

[4] Kim KW, Kim MK, Cho WY. (2019). An analytical model of roll bending steel pipe formed by three rollers. The International Journal of Advanced Manufacturing Technology,104,4039-4048.http://dx.doi.org/10.1007/s00170-019-04183-2.

[5] Xiong H, Ma YN, Zhou SJ, He Y, Yang XN, Jin K, Wang H, Luo XY, Guo XZ. (2018). Free bending forming technology of three dimensional complex axis hollow component. Journal of Plasticity Engineering,25, 100-110. http://dx.doi.org/10.3969/j.issn.2018.01.015.

[6] Zhu YX, Chen W, Tu WB, Guo Y, Chen L. (2019). Three-dimensional finite element modeling of rotary-draw bending of copper-titanium composite tube. The International Journal of Advanced Manufacturing Technology,106,2377-2389. http://dx.doi.org/10.1007/s00170-019-04781-0.

[7] Liu CM, Guo XZ, Huang ZS, Zheng S, Cheng C (2022) The invention relates to a tube fitting forming processing method and forming device for pre-welded bifurcated branch tube. China, CN113020354B.

[8] Jia MH, Wang CL, Sun WH. (2014). Process parameters analysis and mechanical simulation of the tube plastic bending formation. Manufacturing Automation ,36(24),118-122.

[9] Liu HL, Liu YL. (2021). Cross section deformation of heterogeneous rectangular welded tube in rotary draw bending considering different yield criteria. Journal of Manufacturing Processes, 61,303-310.http://dx.doi.org/10.1016/j.jmapro.2020.11.015.

[10] Liu MM, Liu YL, Zhan H. (2019). Forming quality of thin-walled rectangular waveguide tube during small-radius rotary draw bending under different push assistant matching conditions. The International Journal of Advanced Manufacturing Technology, 104,3095-3105.https://doi.org/10.1007/s00170-019-04238-4.

[11] Che Y, Zhan H, Qu JC, Lin J. (2021). Analysis on Instability in Tube Bending Process Based on Total Theory of Plasticity. Journal of Netshape Forming Engineering ,13(3),112-117.https://doi.org/10.3969/j.issn.1674-6457.2021.03.013.

[12] Huang T, Wang K, Zhan M, Guo JQ, Chen XW, Chen FX, Song KX. (2019). Wall Thinning Characteristics of Ti-3Al-2.5V Tube in Numerical Control Bending Process. Journal of Shanghai Jiaotong University (Science), 24(5),647-653.

https://doi.org/10.1007/s12204-019-2079-1.

[13] Fang J, Fang OY, Lu SQ, Wang KL, Min XG. (2021). Effect of process parameters on wall thinning of high strength 21-6-9 stainless steel tube in numerical control bending. Journal of Physics: Conference Series,1885(2). https://doi.org/10.1088/1742-6596/1885/2/022033.

[14] Li GJ, Sun H, Zeng YC, Yang JC, Wang QL, Li H, Wu W. (2021). Research on CNC draw-bending die design for aluminum alloy thin-walled tube with small bending radius. Forging and Stamping Technology, 46(4),150-155. https://doi.org/10.13330 /j.issn. 1000-3940. 2021. 04. 023.

[15] Safdarian R. (2019). Experimental and numerical investigation of wrinkling and tube ovality in the rotary draw bending process. International Journal of Mechanical Sciences, 233(16),5568-5584. https://doi.org/10.1177/0954406219850857.

[16] E DX，Zhou DJ. (2016). Metal Tube Bending: Theory and Forming Defects Analysis. Beijing Institute of Technology press.

[17] Dai K, Wang ZR. (2000). The copamrison between Hencky stress equation and Normal stress equation along the tracing line of principal shera stress. Journal of Materials Processing Technology, (02),27-9.

[18] Fang J, Lu SQ, Wang KL, Min XG. (2016). Effects of Material Mechanical Properties on Wall Thickness Variation in Numerical Control Rotary Draw Bending Process of Tubes. Materials for Mechanical Engineering, 40(4),75-79. https://doi.org/10.11973/jxgcc1201604017.